NOAA Technical Memorandum ERL WPL-140

REMOTE SENSING USING SPATIAL FILTERS: A CASE STUDY

R. J. Lataitis
R. S. Lawrence
S. F. Clifford
D. M. Farmer
G. R. Ochs

Wave Propagation Laboratory
Boulder, Colorado
July 1986

noaa NATIONAL OCEANIC AND ATMOSPHERIC ADMINISTRATION / Environmental Research Laboratories

NOAA Technical Memorandum ERL WPL-140

REMOTE SENSING USING SPATIAL FILTERS: A CASE STUDY

R. J. Lataitis
R. S. Lawrence
S. F. Clifford
D. M. Farmer
G. R. Ochs

Wave Propagation Laboratory
Boulder, Colorado
July 1986

UNITED STATES
DEPARTMENT OF COMMERCE

Malcolm Baldrige,
Secretary

NATIONAL OCEANIC AND
ATMOSPHERIC ADMINISTRATION

Anthony J. Calio,
Administrator

Environmental Research
Laboratories

Vernon E. Derr,
Director

NOTICE

Mention of a commercial company or product does not constitute an endorsement by NOAA Environmental Research Laboratories. Use for publicity or advertising purposes of information from this publication concerning proprietary products or the tests of such products is not authorized.

For sale by the National Technical Information Service, 5285 Port Royal Road
Springfield, VA 22161

CONTENTS

REMOTE SENSING USING SPATIAL FILTERS: A CASE STUDY

R. J. Lataitis, R. S. Lawrence, S. F. Clifford, D. M. Farmer,*

and G. R. Ochs

NOAA/ERL/Wave Propagation Laboratory

Boulder, Colorado 80303

ABSTRACT

The theoretical performance limits of an underwater acoustic profiling system comprising a four-element, equally spaced, linear transmitting and receiving array are investigated. It is found that the turbulence strength can be resolved to roughly 13% of the total path near midpath and 30% near the ends of the path, the useful range of the system lying between 20% and 80% of the total path. The transverse flow velocity measurement is shown to have a shorter range and apparently greater though undeterminable spatial resolution.

1. INTRODUCTION

Lee[1] demonstrated that by using ideal spatial filters, or amplitude weighting functions, on incoherent transmitting and receiving apertures over a line-of-sight propagation path, the received signal could be made sensitive to a single position z_0 along the path and a single spatial wavenumber K_0 of the intervening turbulent refractive index field. He showed that certain characteristics of this spatially filtered signal (e.g., the variance) could be directly related to the mean intensity of the turbulence at a single path position, described by the refractive index structure parameter C_n^2, and others (e.g., the frequency) to the mean transverse flow velocity V at a single path

---

* D. M. Farmer is with the Institute of Ocean Sciences, Sidney, B.C., Canada, V8L 4B2.

position. He pointed out that by changing the relative spatial wavelength of the transmitter and receiver filters, the system could be tuned to different path positions and could, in principle, yield profiles of C_n^2 and V along the path.

Ideal spatial filters are impossible to realize in practice because they have a purely sinusoidal character. Real filters, because of their finite transverse extent and often nonsinusoidal nature within the aperture, can only approximate the ideal case. Therefore, it is not possible to tune a practical profiling system to a single path position and single spatial wavenumber. Such systems are typically sensitive to a narrow part of the path and a band of spatial wavenumbers. They yield mean turbulence intensity profiles that are spatially smoothed versions of the actual profiles and mean velocity profiles that approximate the actual profiles reasonably well though in a non-linear manner.

In this report we investigate the theoretical performance limits of the underwater acoustic profiling system shown in Fig. 1. The transmitter and receiver are linear arrays of four equally spaced elements of diameter D separated by a distance d. The arrays are located at opposite ends of a path of length L and are both oriented along the x-direction. The time series for the log amplitude $\chi = 1/2\ \ell n(p/\langle p\rangle)$, where p and $\langle p\rangle$ are the instantaneous and mean acoustic intensities respectively, and phase ϕ are recorded for each transmitter-receiver pair.[2] (In terms of the in-phase I and quadrature Q components of the received field, $\chi = 1/2\ \ell n[(I^2 + Q^2)/\langle I^2 + Q^2\rangle]$ and $\phi = \tan^{-1}(Q/I)$.) A spatial filter is constructed by assigning a weight α to each transmitter and receiver element. The filtered signals are found from

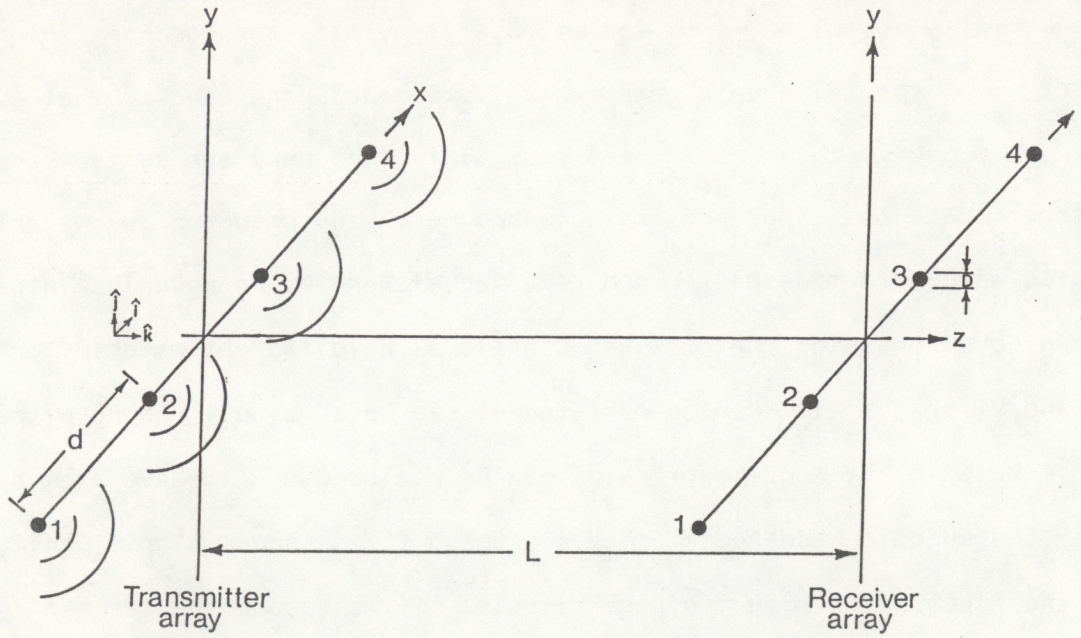

Figure 1. Propagation geometry of an underwater acoustic profiling system.

$$\chi_f(t) = \sum_{i=1}^{4} \sum_{j=1}^{4} \alpha_i \, \alpha_j \, \chi_{i,j}(t) \tag{1a}$$

and

$$\phi_f(t) = \sum_{i=1}^{4} \sum_{j=1}^{4} \alpha_i \, \alpha_j \, \phi_{i,j}(t) , \tag{1b}$$

where the subscripts i and j identify the transmitter and receiver elements respectively. The sum C_f of the filtered log-amplitude covariance function C_{χ_f} and the filtered phase covariance function C_{ϕ_f} (i.e., $C_f(\tau) = C_{\chi_f}(\tau) + C_{\phi_f}(\tau) = \langle[\chi_f(t) - \langle\chi_f(t)\rangle][\chi_f(t+\tau) - \langle\chi_f(t+\tau)\rangle]\rangle + \langle[\phi_f(t) - \langle\phi_f(t)\rangle][\phi_f(t+\tau) - \langle\phi_f(t+\tau)\rangle]\rangle$, where the angle brackets describe ensemble averages) contains information about C_n^2 and V at a given path position z_0 (e.g., the filtered covariance evaluated at zero time lag is the variance σ_f^2 of the filtered signal (i.e., $\sigma_f^2 = C_f(0)$), which is proportional to C_n^2 at z_0; the power spectrum $\tilde{C}(\omega)$ of the filtered signal, defined as the Fourier transform of the filtered

covariance (i.e., $\tilde{C}_f(\omega) \equiv \frac{1}{\pi} \int_0^\infty d\tau \cos(\omega\tau)\, C_f(\tau)$), yields the dominant frequency component ω_0 in the filtered signal, which is linearily related to V at z_0 (i.e., $\omega_0 = K_0 V(z_0)$). Different spatial filters make the system sensitive to different path positions and are obtained merely by changing the weights associated with each transmitter and receiver element as we describe later. Therefore, by processing the received signals using different weights, profiles of C_n^2 and V for the time period of interest can be obtained. We note that the angle brackets in the above expression can be replaced by time averages by invoking the ergodic hypothesis. The averaging times should significantly exceed the fluctuation time τ of the signals. If we assume the largest inhomogeneity in the flow is approximately 3 m, then for V = 1 m/s, $\tau \simeq 3$ s. (The actual signal fluctuation time $\tau \simeq (K_0 V)^{-1}$ will be shorter than this.)

The remaining sections in this report are organized as follows. Section 2 contains a geometric interpretation of spatial filtering that provides some insight into what weights are needed to obtain a particular path weighting function (i.e., the function that describes the sensitivity of the system as a function of path position), and helps the reader gain some feeling for how spatial filtering works. In Section 3 a general equation for the filtered covariance is presented. Section 4 investigates aperture averaging effects that result from the finite size of each transmitting and receiving element. Sections 5 and 6 describe various C_n^2 and velocity profiling techniques respectively. The conclusions are presented in Section 8.

Certain assumptions have been made to simplify the analysis in this report. Perhaps the most important is the requirement that the scattering be weak and that the narrow-angle approximation apply.[3] The turbulence has been treated as

locally homogeneous and isotropic, and is assumed to be advected across the path by the mean flow, which is assumed to have a component along the array axis only. The transmitter and receiver arrays are considered incoherent, the element weights in each array satisfying $\Sigma\alpha = 0$. This latter requirement removes any sensitivity of the array to the lowest wavenumber components of the refractive index spectrum, which tend to broaden the path weighting functions (i.e., reduce the spatial resolution).

2. GEOMETRIC INTERPRETATION OF SPATIAL FILTERING

A geometric method for describing the concept of spatial filtering is illustrated in Figs. 2a and 2b. Figure 2a depicts an eight-element, linear transmitting and receiving array separated by a distance L whose elements have alternating weights of +1 and -1. (We chose eight-element arrays instead of four because it is easier to illustrate the relevant ideas.) Note that the vertical scale is greatly expanded relative to the horizontal. The lines connecting the elements identify the lines-of-sight between all the transmitter-receiver pairs. A nodal structure is clearly present in the center of the pattern. The number at each of the nodes represents the excess weight there calculated by multiplying the weights of each transmitter-receiver pair that has a line of sight through that node, and summing the result. The presence of such a nodal structure is interpreted as a point of increased sensitivity along the path. The spacing between the nodes and the alternating nature of the excess weights determines the resonant spatial wavenumber. The modulation amplitude of these weights describes the magnitude of the response at that path position. The inferred path weighting function is given directly below the figure. In terms of the spatial wavelength of the transmitter (K_t) and receiver (K_r) array,

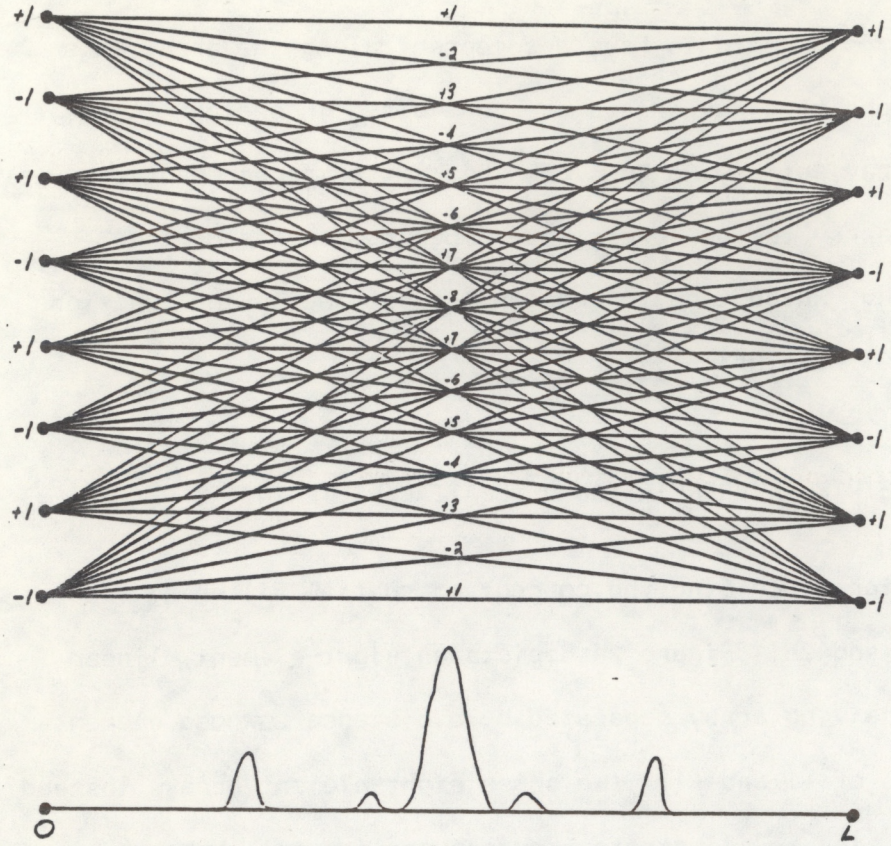

Figure 2a. (Top) A geometric interpretation of spatial filtering for an eight-element transmitter and receiver array with equal spatial wavenumbers and (bottom) the inferred path weighting function.

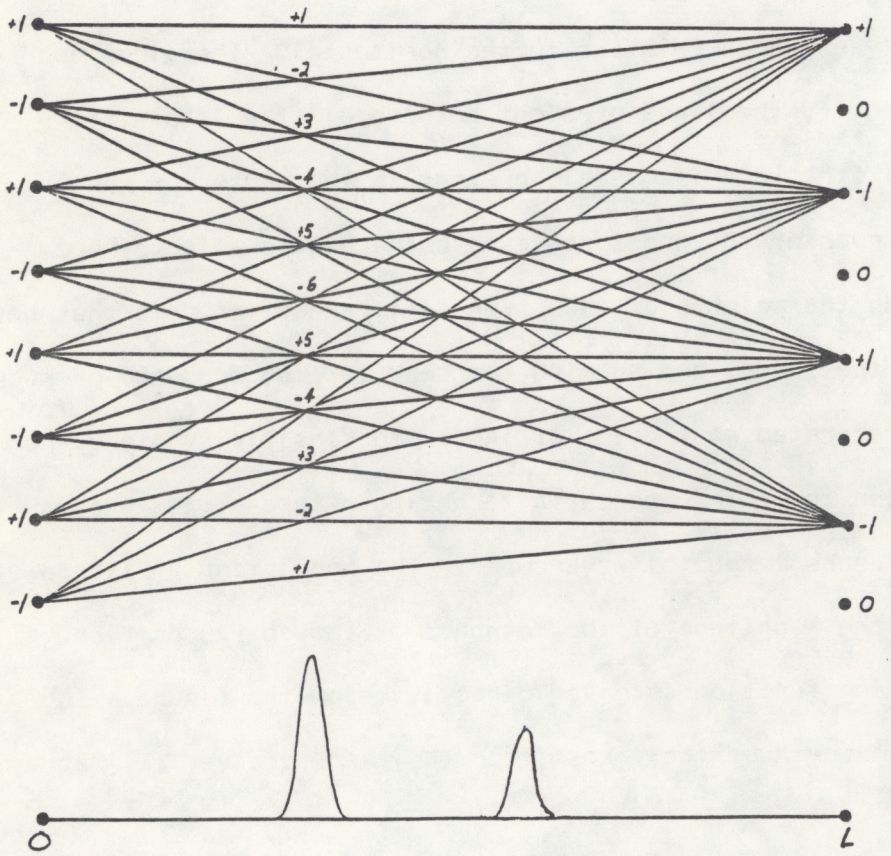

Figure 2b. (Top) A geometric interpretion of spatial filtering for an eight-element transmitter and receiver array with unequal spatial wavenumbers and (bottom) the inferred path weighting function.

which for this case satisfies $K_t = K_r$, this approach indicates that the maximum path sensitivity occurs at $z_0 = L/2$, and the resonant wavenumber K_0 satisfies $K_0 = 2K_t = 2K_r$. Lee[1] predicts $z_0 = L(1 + K_t/K_r)^{-1} = L/2$ and $K_0 = K_t + K_r$, which agrees with this geometric approach. The presence of the additional regions of sensitivity or sidelobes is due to the presence of higher order spatial harmonics in the element weighting functions. These can be eliminated in principle by choosing the weights to model more accurately a sinusoidal modulation. In this discussion we neglected the influence of the refractive index spectrum, which for turbulence described by a Kolmogorov spectrum would attenuate the contributions from the higher spatial wavenumbers and generally reduce the size of the sidelobes.

Figure 2b demonstrates how the system can be tuned to a different path position by changing the weights in such a way as to change the relative spatial wavelengths of the filters. For this case we have $K_t = 2K_r$, and Lee predicts $z_0 = L/3$ and $K_0 = 3/2\ K_t = 3K_r$, which also agrees with the geometric approach.

To see how well this technique agrees with a numerical calculation, we evaluated the corresponding path weighting functions for a four-element transmitting and receiving array and obtained the results shown in Figs. 3a and 3b. A refractive index spectrum with a -11/3 power law was used to obtain these results. The overall agreement is reasonable, demonstrating the utility of this geometric approach for predicting the peak positions in the path weighting functions without going through extensive calculations and also as an aid to understanding the mechanism behind spatial filtering. We note that this method does not give any information about the obtainable spatial resolution.

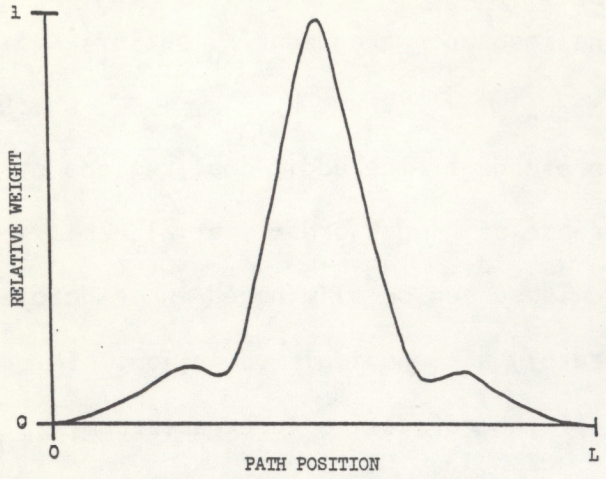

Figure 3a. The path weighting function for a four element transmitter and receiver array with equal spatial wavenumbers, assuming a refractive index spectrum with a -11/3 power law.

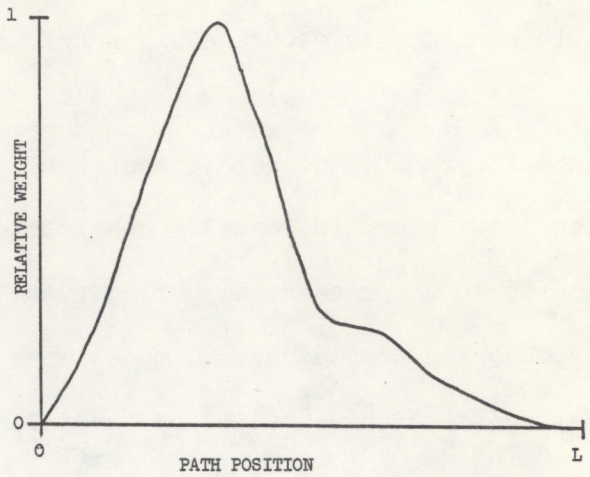

Figure 3b. The path weighting function for a four element transmitter and receiver array with a spatial wavelength ratio of two assuming a refractive index spectrum with a -11/3 power law.

3. GENERAL EQUATIONS FOR SPATIALLY FILTERED SIGNALS

Figure 4 illustrates a general configuration for a profiling system using a single spatially filtered transmitter and two spatially filtered receivers of arbitrary cross section. Information about the mean turbulence intensity and mean flow velocity across the path is contained in the filtered covariance function C_f (i.e., the sum of the log-amplitude and phase covariance function) given by Lee[1] as

$$C_f(\vec{\rho},\tau) = 2\pi k^2 L \int_0^1 du \int d^2\vec{K}\, \Phi_n(\vec{K},0,u)\, e^{i\vec{K}\cdot(\vec{\rho}u - \vec{V}\tau)} \times$$

$$\times \left|F_t[\vec{K}(1-u)]\right|^2 \left|F_r(\vec{K}u)\right|^2 , \qquad (2)$$

where $\vec{\rho}$ is a transverse vector connecting the centers of two receiver arrays, τ is a time delay, k is the acoustic wavenumber, u is the normalized path position, and $\vec{K}$ is the transverse wavenumber of the refractive index spectrum Φ_n. The factors F_t and F_r in Eq. (2) are the two-dimensional Fourier transforms of

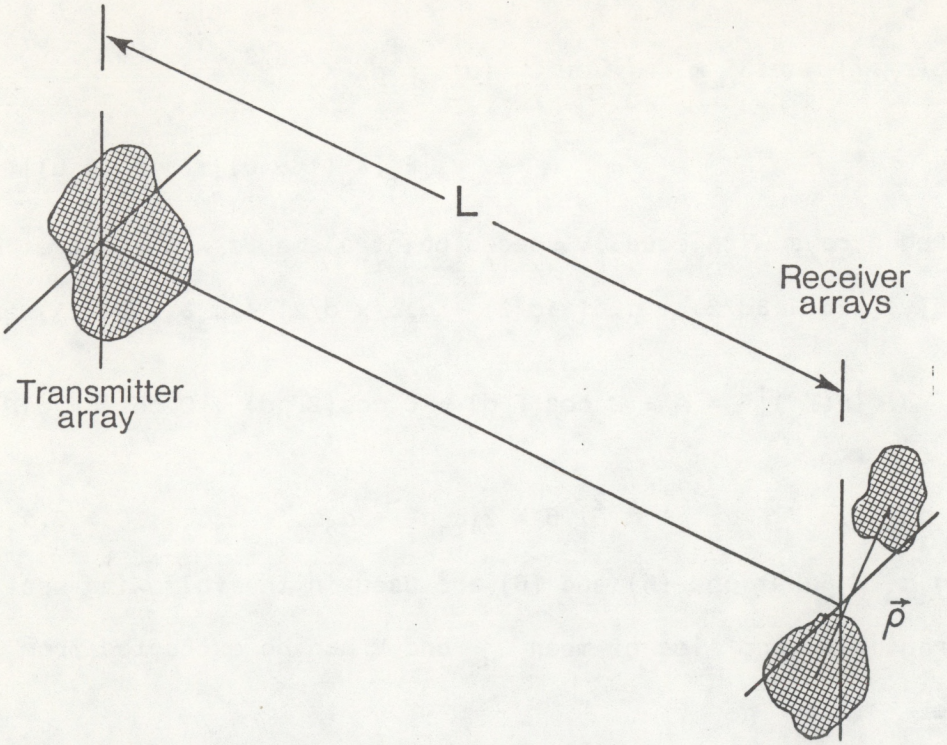

Figure 4. A general configuration for a profiling system using spatially filtered apertures with arbitrary cross sections.

the aperture amplitude weighting functions f_t and f_r respectively and are defined through

$$F(\Gamma_x,\Gamma_y) = \int_{-\infty}^{\infty}\int_{-\infty}^{\infty} dx\, dy\, e^{i(\Gamma_x x + \Gamma_y y)} f(x,y) \ , \qquad (3)$$

where Γ_x and Γ_y are the spatial wavenumbers of the aperture weighting functions along the x and y directions respectively. For linear arrays with point elements that lie along the x-axis as shown in Fig. 1, F will be a function only of Γ_x. Assuming $\vec{\rho} = \rho_x \hat{i}$ and $\vec{V} = V\hat{i}$, where $\hat{i}$ is a unit vector in the x-direction, and using the following form for the refractive index spectrum,

$$\Phi_n(\vec{K},0) = \Phi_n(K_x,K_y,0) = 0.033\, C_n^2(u)\, (K_x^2 + K_y^2)^{-11/6} \ , \qquad (4)$$

Eq. (2) reduces to

$$C_f(\rho_x,\tau) = 0.35\, k^2 L \int_0^1 du\, C_n^2(u) \int_{-\infty}^{\infty} dK_x K_x^{-8/3}\, e^{iK_x(\rho_x u - V\tau)} \times |F_t[K_x(1-u)]|^2\, |F_r(K_x u)|^2 . \quad (5)$$

For centered arrays with equally spaced point elements with separation d, $f(x,y) = \delta(y)[\alpha_1\delta(x+3d/2) + \alpha_2\delta(x+d/2) + \alpha_3\delta(x-d/2) + \alpha_4\delta(x-3d/2)]$ and

$$|F(\Gamma_x)|^2 = A + B\cos(\Gamma_x d) + C\cos(2\Gamma_x d) + D\cos(3\Gamma_x d) , \quad (6)$$

where $A = \alpha_1^2 + \alpha_2^2 + \alpha_3^2 + \alpha_4^2$, $B = 2(\alpha_1\alpha_2 + \alpha_2\alpha_3 + \alpha_3\alpha_4)$, $C = 2(\alpha_1\alpha_3 + \alpha_2\alpha_4)$, and $D = 2\alpha_1\alpha_4$. Equations (5) and (6) are used in the following sections to show how, in principle, profiles of mean C_n^2 and V can be extracted from the filtered covariance.

4. THE EFFECT OF APERTURE AVERAGING

In Section 3 we presented a general equation for the space-time covariance of a spatially filtered signal. This was reduced for the specific case of linear arrays of point elements. For finite elements, the equation becomes much more complex. To study the effect of aperture averaging without significantly increasing the complexity of the equation, we consider elements that have a finite width D in the x-direction only. The amplitude weighting is assumed constant over the width of each element. If we assume the element apertures are incoherent, the only modification to the previous results is a factor $\mathrm{sinc}^2(\Gamma_x D/2)$ that multiplies the right side of Eq. (6). This result is not surprising because the aperture averaging factor in wavenumber space for an incoherent aperture is the square of the Fourier transform of the amplitude weighting function for that aperture.[4] (The element apertures are actually

coherent; however, if their diameters are much smaller than the first Fresnel zone $\sqrt{L/k}$, the aperture averaging factor is the same as that for incoherent apertures[5].)

To quantify the impact of aperture averaging, we examine the effect of finite element width on the determination of C_n^2. The filtered variance (i.e., the sum of the variance of the filtered log-amplitude and phase time series) is given by Eq. (5) as

$$\sigma_f^2 = C_f(0,0) = \int_0^1 du\, C_n^2(u)\, W(u) \,, \tag{7a}$$

where W(u) is the path weighting function defined by

$$W(u) = 0.700\, k^2 L d^{5/3} \int_0^\infty dS\, S^{-8/3}\, |F_t[S(1-u)]|^2\, |F_r(Su)|^2 \,, \tag{7b}$$

$S = K_x d$ being a normalized wavenumber. The point and finite element path weighting functions for a four element transmitting and receiving array with element weights of (+1, -1, +1, -1) and $\alpha = d/D = 4$ are shown in Fig. 5. The two curves differ slightly in total area and sidelobe emphasis. The area under the two curves differs by approximately 5%, which corresponds to an aperture averaging error of 5% if the point element results [Eq. (6)] were used to estimate C_n^2 (see Section 5). We expect this error to decrease as α increases for the following reason. The resonant spatial wavenumber K_0 is roughly $2\pi/d$, where d is the spacing between the elements. The characteristic size of the disturbance at the receiving array produced by this Fourier component is approximately d. Aperture averaging effects become less important as the diameter D of the receivers decreases relative to the size d of the disturbance at the receiver array; that is, aperture averaging effects decrease as α increases. Therefore provided $\alpha = d/D > 4$, aperture averaging effects will account for less than 5%

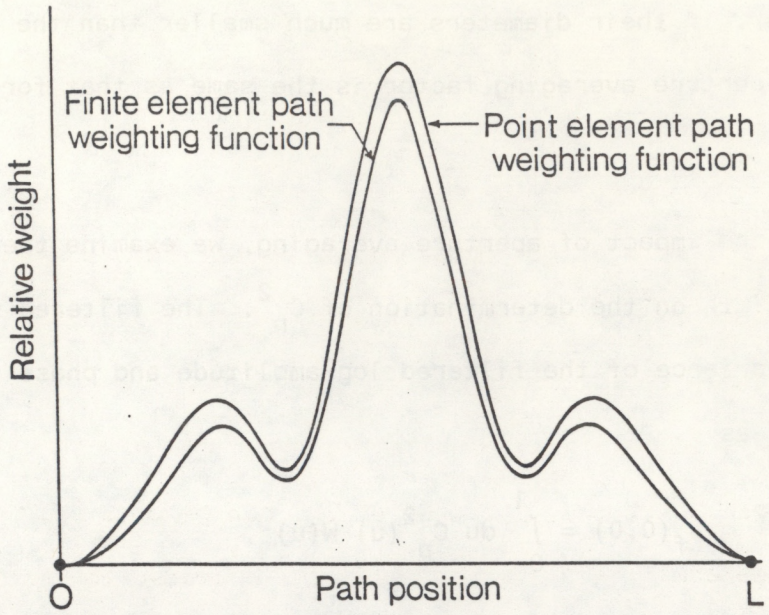

Figure 5. The point and finite element path weighting function for a four-element transmitter and receiver array with weights of (+1,-1,+1,-1) and $\alpha = d/D = 4$.

of the total error in the retrieved C_n^2 values. We note that it may be possible to compensate for this error by adjusting the estimated C_n^2 values for a given α and a given set of element weights. However, in what follows we assume $\alpha > 4$ and use the point element theory.

5. C_n^2 PROFILING

Profiles of C_n^2 are obtained from the filtered variance σ_f^2 by using Eq. (7a). A particular combination of element weights produces a path weighting function with a center-of-gravity at u_c and a peak at u_p. These are evaluated numerically using Eq. (7b). We propose two methods for estimating C_n^2. In the first we assume that the path-integrated contribution to σ_f^2 originates entirely at u_c and estimate C_n^2 there by using Eq. (7a) to obtain

$$C_n^2(u_c) \simeq A'^{-1} \sigma_f^2 , \qquad (8)$$

where $A' = \int_0^1 du\, W(u)$. That is, the filtered variance σ_f^2 is found from the experimental data for a given set of element weights that correspond to a computed path weighting function with center-of-gravity u_c, and then Eq. (8) is used to estimate C_n^2 at u_c. (We note that A' in Eq. (8) is the product of the normalization factor and normalized area A in Tables 1 and 2b.) The second approach is identical to the first except that we replace u_c by u_p. By changing the element weights to obtain path weighting functions with a different centers-of-gravity and peak positions, profiles of C_n^2 can be obtained. These two methods will in general yield similar profiles, provided the path weighting functions are reasonably symmetric.

The normalized path weighting functions shown in Fig. 6 were obtained from Eq. (7b) after using the geometric method described in Section 2 to arrive at a reasonable set of element weights and then adjusting them to obtain the best resolution. These adjustments included tapering the weights at the ends of the arrays to minimize the effect of the finite array lengths and also computing the Fourier series associated with a given set of weights and then adjusting the weights to maximize the coefficient of the desired Fourier component. Table 1 describes the characteristics of the filters and the corresponding path weighting functions shown in Fig. 6.

The resolution R associated with each filter is defined as the ratio of the path length to the width of the path weighting functions at a relative weight of 0.5, and is shown in the last column of Table 1. A higher resolution number corresponds to a narrower path weighting function and a greater spatial resolution. Note that the resolution R defined in this manner is not an absolute resolution but is a relative resolution compared with the total path length.

Table 1.--The normalization factor, element weights, center-of-gravity u_c, peak position u_p, normalized area A, and resolution R of the direct filter normalized path weighting functions shown in Fig. 6.

Normalized path weighting function	Normalization factor	Transmitter weights				Receiver weights				u_c	u_p	A	R
1	3.02	-.4	1	-1	.4	-1	-.5	.5	1	0.32	0.26	0.30	4.0
2	1.68	-.4	1	-1	.4	0	-1	0	1	0.36	0.32	0.35	3.6
3	2.42	.1	-1	1	-.1	1	-1	-1	1	0.47	0.40	0.43	2.6
4	1.87	.5	-1	1	.5	.5	-1	1	.5	0.50	0.50	0.24	5.7
5	2.42	1	-1	-1	1	.1	-1	1	-.1	0.53	0.60	0.43	2.6
6	1.68	0	-1	0	1	-.4	1	-1	.4	0.64	0.68	0.35	3.4
7	3.02	-1	-.5	.5	1	-.4	1	-1	.4	0.68	0.74	0.30	4.0

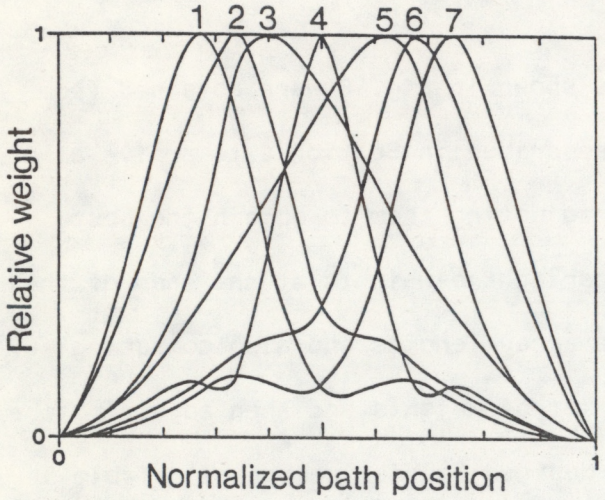

Figure 6. Direct filter normalized path weighting functions for a four-element transmitter and receiver array with the element weights shown in Table 1, as a function of the normalized path position.

The width of the path weighting function in percent of the total path is given by 100 R^{-1}. The seven path weighting functions shown in Fig. 6, corresponding to the seven sets of element weights shown in Table 1, allow us to obtain spatially averaged information about C_n^2 at seven different positions, either at the centers-of-gravity of each path weighting function or the peaks, depending on which method is chosen. The resolution is a strong function of the position along the path and depends on the number of spatial cycles in the length of the

arrays and how well the element weighting functions represent a pure sinusoid, which can be determined by computing the Fourier series of the element weighting function and looking at the relative sizes of the Fourier coefficients remembering that the higher wavenumber components are attenuated by the refractive index spectrum. We find that the resolution of the path weighting functions near the ends and the center of the path is dominated by the number of spatial cycles in the array. The resolution of those with peaks at 0.4 and 0.6 is dominated by the higher order spatial harmonics in the element weighting functions that could not be eliminated without shifting the peaks away from the desired positions.

The path weighting functions shown in Fig. 6 indicate that using the peak position of the path weighting function spatially averaged information about C_n^2 can be obtained from 25% to 75% of the total path with a spatial resolution that varies roughly from 20% to 40% of the total path. This is reasonably good for a system comprising only four transmitter and receiver elements. We have attempted to obtain better resolution by using a method that involves subtracting a fraction of one path weighting function from another which utilizes the finestructure present in each of the weighting functions. Experimentally, this corresponds to calculating the filtered variance for two sets of element weights and subtracting one from the other according to a prescribed rule. The path weighting functions in Fig. 7 were obtained by randomly generating a set of 100 path weighting functions and then randomly subtracting one from a fraction of another and correlating the result with a δ-function at some desired path position. The path weighting function chosen for a particular position was the one that yielded the highest correlation with the δ-function at that path position. Table 2a contains the transmitter and receiver element weights of the individual

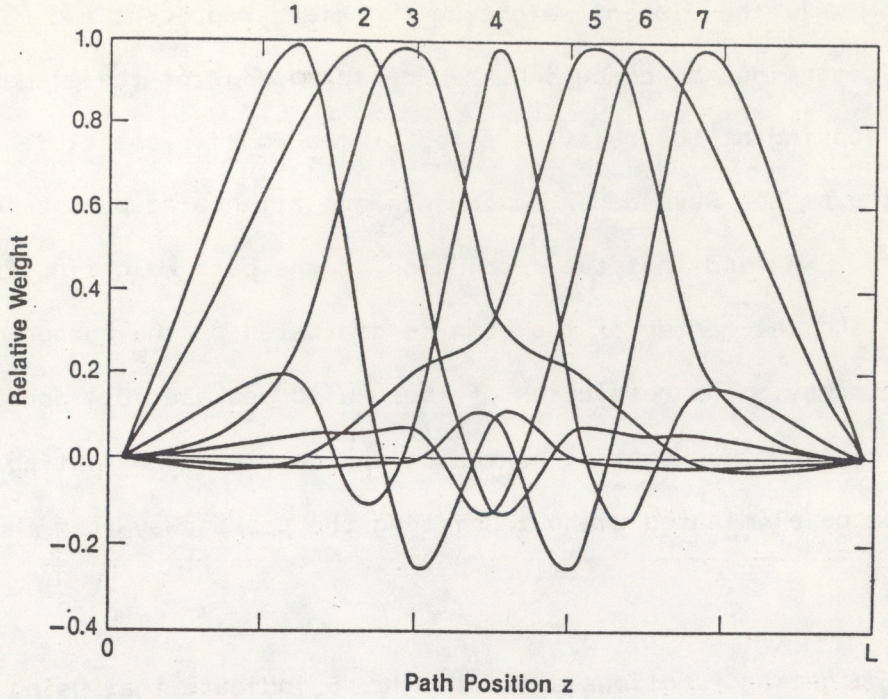

Figure 7. Combination filter normalized path weighting functions for a four-element transmitter and receiver array obtained by combining the path weighting functions of the individual filters with the element weights shown in Table 2a according to the rule given in Table 2b.

filters used to form the combination filters corresponding to the path weighting functions shown in Fig. 7. Table 2b describes the characteristics of the combination filters and gives the rule for obtaining each path weighting function from the individual filters. Using these combination filters with the center-of-gravity method for estimating C_n^2, we can obtain spatially averaged C_n^2 profiles from roughly 20% to 80% of the total path with a spatial resolution that varies from 13% to 25%. This represents a significant improvement over the previous set of path weighting functions. Another advantage to this method is that it produces path weighting functions whose tails oscillate about zero, which, for reasonably smooth C_n^2 profiles, tends to minimize the influence of refractive index fluctuations that occur away from the region of interest. One

Table 2a.--The transmitter and receiver weights and area A' under the corresponding path weighting function of the individual filters used to obtain the path weighting functions shown in Fig. 7.

Filter	Transmitter weights				Receiver weights				A'
a	.28	.45	-.45	-.28	.68	-.98	.98	-.65	0.24
b	.60	-.63	.63	-.60	.91	-.20	.20	-.91	0.52
c	.35	.80	-.80	-.35	.21	-.30	.30	-.21	0.06
d	.94	.82	-.82	.94	.89	.84	-.84	.89	1.11
e	-.26	-.57	.57	.26	.77	-.55	.55	-.77	0.37
f	.12	-.62	.62	-.12	-.21	-.96	.96	.21	0.20
g	.83	.26	-.26	.83	.08	.98	-.98	-.08	0.72
h	-.89	-.14	.14	.89	.45	-.80	.80	-.45	0.43

Table 2b.--The normalization factor, combination rule, center-of-gravity u_c, peak position u_p, normalized area A, and resolution R of the combination filter normalized path weighting functions shown in Fig. 7.

Normalized path weighting function	Normalization factor	Combination rule	u_c	u_p	A	R
1	0.37	0.76hR - 1.11aR (*)	0.17	0.24	0.167	5.45
2	0.47	7.44cR - 0.43gR	0.29	0.32	0.243	4.33
3	0.63	2.38f - 0.61b	0.39	0.38	0.237	5.12
4	0.69	0.29d - 0.97e	0.49	0.50	0.167	8.05
5	0.63	2.38fR - 0.61bR	0.61	0.62	0.237	5.12
6	0.47	7.14c - 0.43g	0.71	0.68	0.243	4.33
7	0.37	0.76h - 1.11a	0.83	0.76	0.167	5.45

(*) R means that the transmitter and receiver element weights are interchanged.

possible problem with this approach is that the subtraction process may result in an intolerably low SNR. In the Appendix we calculate the expected SNR for the direct filters described in Fig. 6 and Table 1, and the combination filters described by Fig. 7 and Table 2b. We include the effect of finite averaging times and the SNR of each transmitter-receiver pair. Our calculations show the

minimum SNR to be around 13.3 dB for the direct filters and 3.5 dB for the combination filters, which indicates that for the least favorable configuration (i.e., the one which produces the smaller variance) the combination filters may be only marginally useful.)

To demonstrate the profiling potential of such a system, we chose a mean C_n^2 profile and attempted to retrieve it by integrating it against the seven path weighting functions shown in Fig. 7. The results of this simulation are shown in Fig. 8. The seven points represent the C_n^2 estimates at the center-of-gravity of each of the seven path weighting functions. The retrieved profile is the best least-squares fit of a fourth order polynomial to these points and was obtained by integrating the assumed profile against the path weighting functions to obtain a singly retrieved profile, repeating this procedure with the singly retrieved profile to obtain a doubly retrieved profile, and then taking the difference between the two and applying it in the opposite sense to the singly retrieved profile. This helps compensate for some of the inherent spatial averaging. The retrieved profiles are spatially smoothed versions of the actual profiles and compare well with the assumed profiles, provided the mean C_n^2 variations are reasonably smooth. Clearly the system will have difficulty in retrieving abrupt changes in the profiles.

6. FLOW VELOCITY PROFILING

Velocity information is obtained from the sum of the power spectra of the filtered log-amplitude and phase time series which is given by the Fourier transform of Eq. (5),

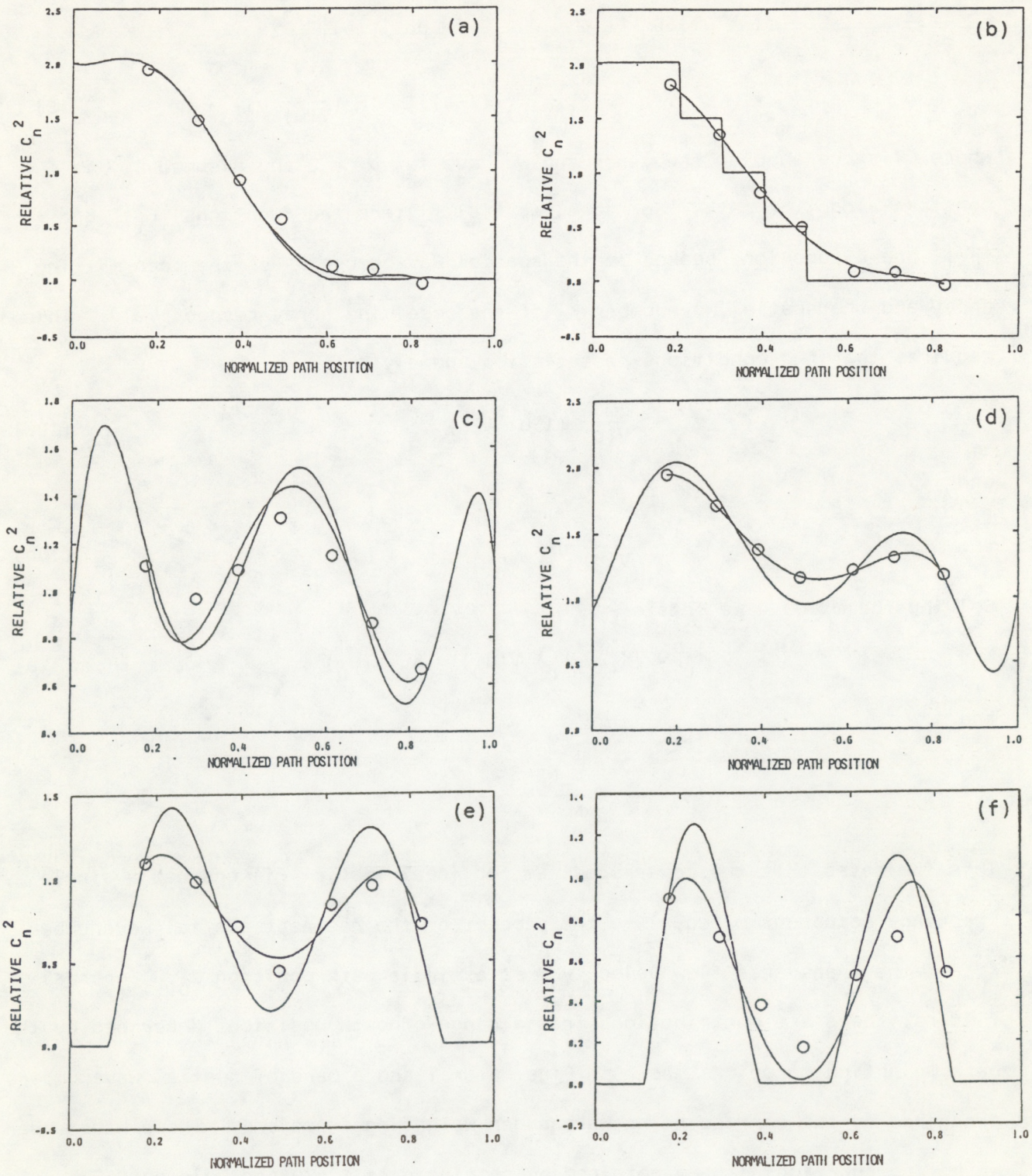

Figure 8. Assumed mean C_n^2 profiles and the retrieved profiles using the center-of-gravity method with the difference filters whose path weighting functions are shown in Fig. 7. Each figure corresponds to a different assumed C_n^2 profile.

$$C_f(\omega) = 0.350\ k^2 L\ \omega^{-8/3}\ C_n^2 \int_0^1 du\ |V(u)|^{5/3} \times$$

$$\times\ |F_t[\frac{\omega}{V(u)}\ (1-u)]|^2\ |F_r(\frac{\omega}{V(u)}\ u)|^2\ , \qquad (9)$$

where ω is the angular frequency and we have set $\rho_x = 0$ and assumed C_n^2 is constant along the path. For ideal spatial filters the functions $|F_t|^2$ and $|F_r|^2$ are δ-functions peaked at the spatial wavenumber K_t of the transmitting array and the spatial wavenumber K_r of the receiving array respectively. This requires that two conditions be satisfied; namely

$$\frac{\omega}{V(u)}\ (1-u) = K_t\ , \qquad (10a)$$

and

$$\frac{\omega}{V(u)}\ u = K_r\ . \qquad (10b)$$

Solving for ω and u we obtain

$$\omega_0 = (K_t + K_r)\ V(u_0) = K_0\ V(u_0)\ , \qquad (11a)$$

and

$$u_0 = \frac{K_r}{K_t + K_r} = \frac{z_0}{L}\ . \qquad (11b)$$

This indicates that the power spectrum for ideal spatial filters has a single frequency component ω_0 equal to the product of the resonant spatial wavenumber K_0 and the transverse flow velocity V at a single path position z_0. For real filters, there are contributions from a range of path positions described by the path weighting functions shown in Figs. 6 or 7 and a band of spatial wavenumbers described by the corresponding wavenumber weighting functions. These wavenumber weighting functions can be obtained by setting $\rho_x = \tau = 0$ and holding C_n^2 constant in Eq. (5), and interchanging the u and K_x integrals to obtain

$$\sigma_f^2 = C_f(0,0) = \int_0^\infty dS\ W(S)\ , \tag{12a}$$

where

$$W(S) = 0.70\ k^2 L\ C_n^2\ d^{5/3}\ S^{-8/3} \int_0^1 du\ |F_t[S(1-u)]|^2\ |F_r(Su)|^2 \tag{12b}$$

is the wavenumber weighting function, $S = K_x d$ being a normalized wavenumber. Figures 9 and 10 show W(S) for the direct filters, described by Fig. 6 and Table 1, and the difference filters, described by Fig. 7 and Tables 2a and 2b, respectively. They indicate that a system using the direct filters will be sensitive to a reasonably narrow band of spatial wavenumbers whereas the one using the combination filters will, in some cases, have contributions from a broader band of wavenumbers or even a few dominant wavenumbers (Figs. 10c and 10d respectively). This poses a problem for retrieving velocity information because the corresponding frequency spectrum may be relatively broad with an unresolvable peak or may have more than one peak thus increasing the likelihood that the frequency spectrum is significantly influenced by the flow velocity at more than one path position. At this stage in the development, the direct filters appear to be the only practical choice for retrieving velocity profiles.

Figure 11 shows a numerical simulation of a velocity profile measurement for the direct filters described in Table 1. The solid line is the assumed profile and the circles represent the retrieved velocity values at the peaks in the seven path weighting function shown in Fig. 6. The estimated velocity values were obtained by locating the peak u_0 and S_0 in the path and wavenumber weighting functions respectively and the peak Ω_0 in the corresponding frequency spectrum and then using $\Omega_0 = S_0\ f(u_0)$ to obtain the velocity estimate at u_0, where Ω_0 is a normalized frequency and f(u) is a normalized velocity defined

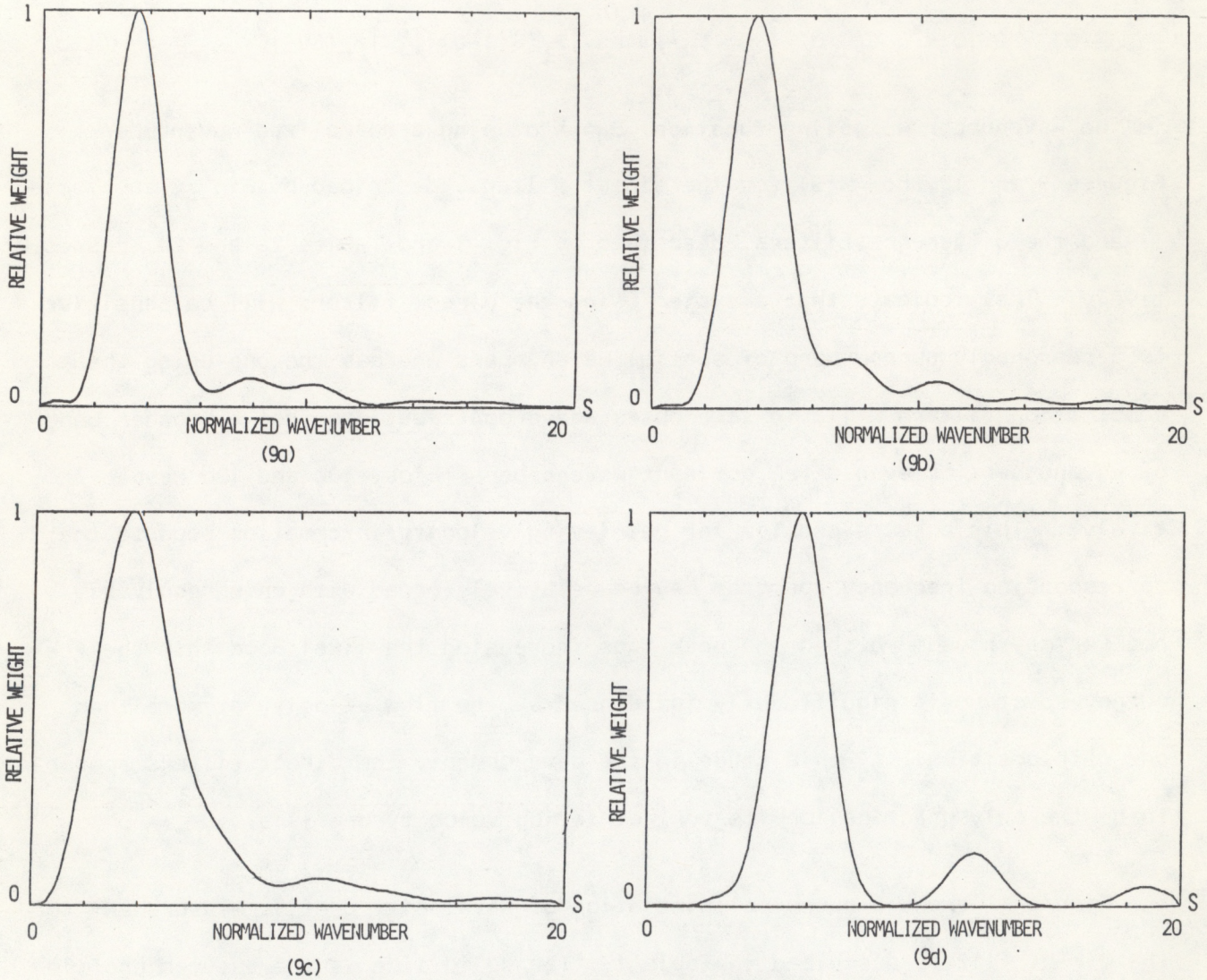

Figure 9. The wavenumber weighting functions corresponding to the direct filters described by Fig. 6 and Table 1. Figures 9a, 9b, 9c, and 9d correspond to filter numbers 1 and 7, 2 and 6, 3 and 5, and 4 respectively. Their peaks occur at S - 3.50, 3.90, 3.60, and 5.70 respectively.

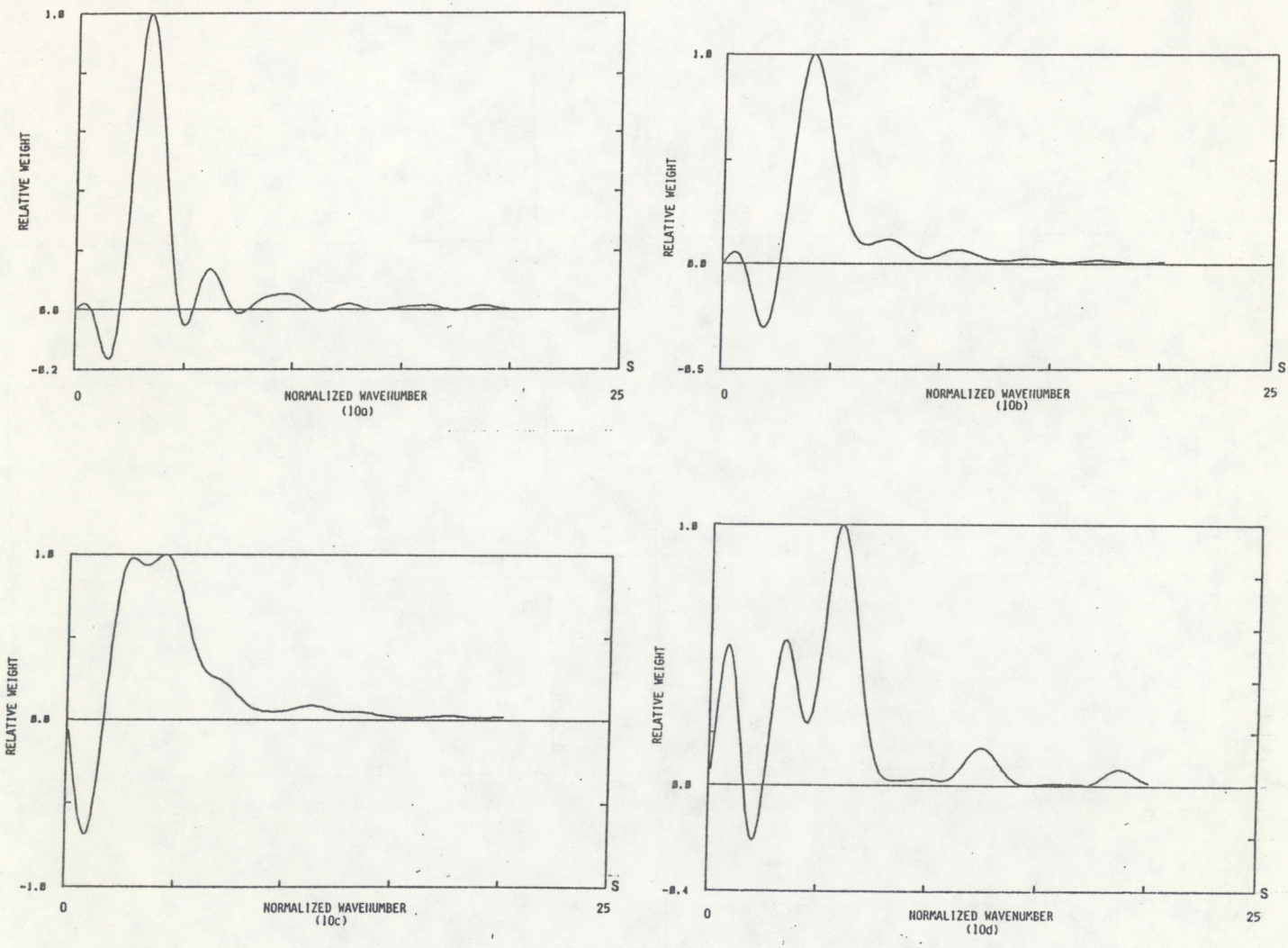

Figure 10. The wavenumber weighting functions for the combination filters described by Fig. 7 and Tables 2a and 2b. Figures 10a, 10b, 10c, and 10d correspond to filter numbers 1 and 7, 2 and 6, 3 and 5, and 4 respectively.

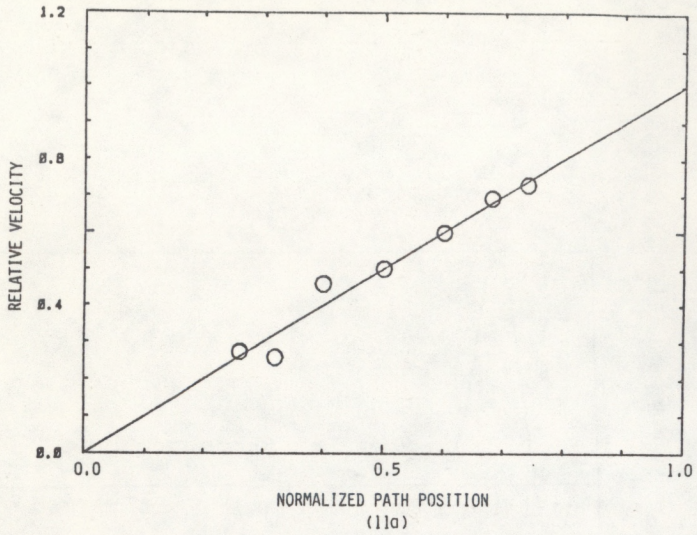

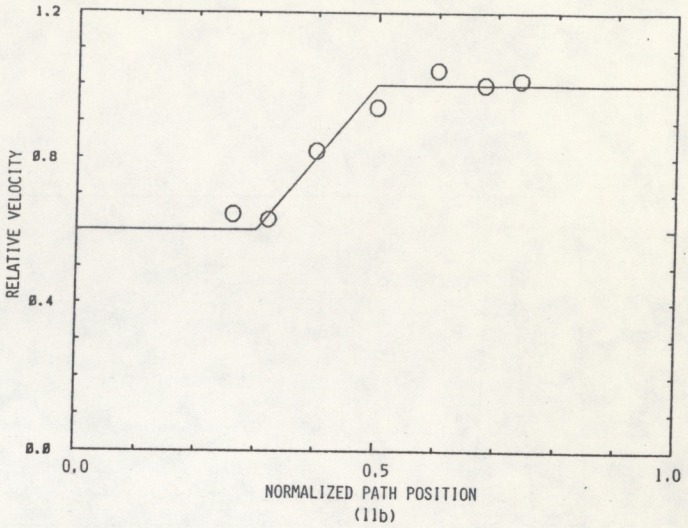

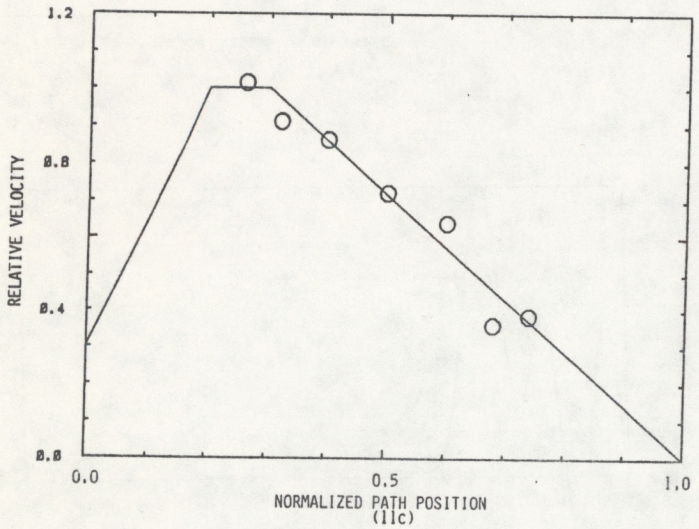

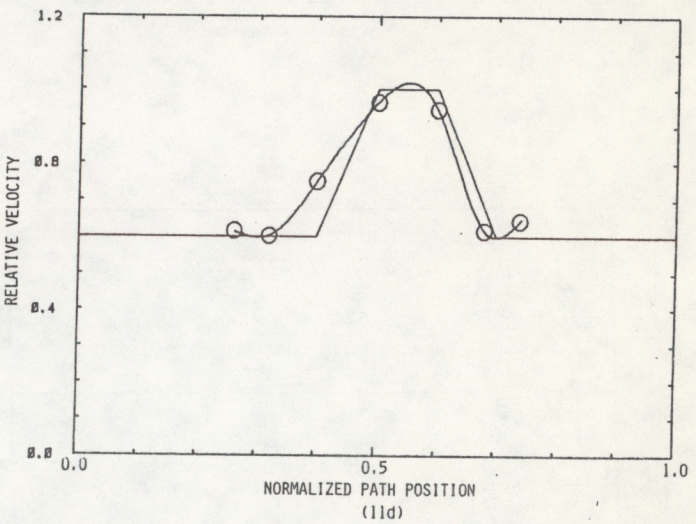

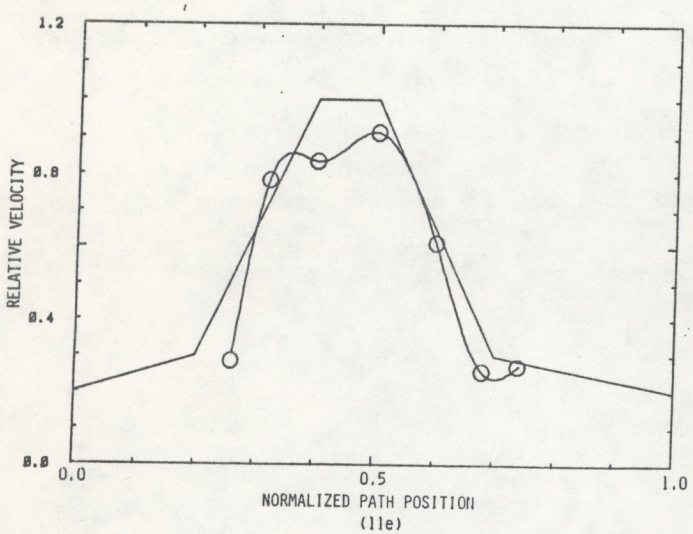

Figure 11. The assumed velocity profile (solid line) and retrieved values (circles) using the seven direct filters described in Table 1. The line through the retrieved values in Figs. 11d and 11e represents a cubic spline fit. Each figure corresponds to a different assumed velocity profile.

through $V(u) = V_0\, f(u)$. (An alternative method is to use the centers of gravity instead of peak positions.) The frequency spectrum, in terms of the normalized frequency Ω, can be obtained from Eq. (9) and is given by

$$C_f(\Omega) \propto \Omega^{-8/3} \int_0^1 du\, |f(u)|^{5/3}\, \left|F_t\left[\frac{\Omega}{f(u)}\,(1-u)\right]\right|^2 \times$$

$$\times \left|F_r\left[\frac{\Omega}{f(u)}\,u\right]\right|^2 . \qquad (13)$$

Experimentally one would locate the peak ω_0 in the frequency spectrum and equate it with $S_0\, V(u_0)/d$, which can be solved for the velocity V. There is a surprisingly good agreement between the assumed and retrieved profiles. One reason may be that the peak temporal frequency is produced solely by the dominant spatial wavenumber at the dominant path position. The contribution from the other path positions and wavenumbers apparently tends to broaden the temporal frequency spectrum without significantly changing the location of the peak, which is at essentially the same position were ideal filters used. By looking at the retrieved velocity values we see that the spatial averaging that was so evident in the retrieved C_n^2 profiles is not so evident in the retrieved velocity profiles, which tends to support the above interpretation. The scatter of the retrieved points about the assumed profile is not predictable and reflects the nonlinearity of the relationship between the velocity profile and frequency spectrum that is evident in Eq. (13). These factors make it difficult to associate a spatial resolution with the velocity measurement. We can only say that, for the velocity profiles tested, the spatial resolution appears to be greater than for the C_n^2 measurement. The solid lines drawn through the velocity estimates in Fig. 11d and 11e represent a cubic spline fit.

One drawback of this method is that it cannot predict the flow direction. A possible solution is to form the time-lagged, log-amplitude and phase covariance

functions for a single-source, two receiver configuration, and for a single-receiver, two-source configuration. The slope at zero lag of the sum of the log-amplitude and phase covariance functions (which is equivalent to the structure function of Farmer and Clifford[6]) is directly proportional to the transverse flow velocity with a path weighting of $u^{2/3}$ and $(1-u)^{2/3}$ respectively, where u is the normalized path position.[6] The path weighting is independent of the separation between the two receivers or the two sources. The flow direction can be inferred from the sign of the slope of this summed covariance function at zero lag. This method will give a path-averaged flow direction over a region near the transmitter or receiver depending on which configuration is used. The wind direction averaged over the middle part of the path can be obtained from the sign of the slope at zero lag of the log-amplitude covariance of two receivers separated by approximately $0.3\sqrt{\lambda L} \simeq 1.2$ m.[7] Greater resolution in the flow direction measurement requires spatial filtering techniques that involve all the transmitters and receivers. For example the signals from two laterally displaced receiver arrays can be used to form a filtered time-lagged covariance function sensitive only to a narrow region of the path. However, this opens the possibility to a host of new techniques for extracting velocity profiles that are beyond the scope of this report.

7. SUMMARY

Our analysis indicates that a profiling system comprising a four element transmitting and receiving array can retrieve profiles of the mean C_n^2 and flow velocity V along a propagation path with reasonable accuracy. The range of the systems varies from approximately 20% to 80% of the total path with a spatial resolution of roughly 20% to 30% for the C_n^2 profiles and a shorter range but greater though undetermined resolution for the velocity profiles.

We have neglected several factors that might reduce the accuracy with which profiles can be retrieved. The first concerns the dependence of the velocity profiling technique on the vector nature of the flow. If, however, we know in advance that the flow is primarily along the array axis, which we assume to be the case in our development, uncertainties due to other components of the flow are small and can be neglected. We have also neglected the uncertainty in the flow estimates due to C_n^2 fluctuations along the path. These present a problem but can be minimized by using the retrieved C_n^2 profile in the flow velocity calculations.

There are a variety of other velocity probing techniques[4] that lend themselves to spatial filtering concepts. For instance the normalized slope at zero lag of the filtered covariance function which is related to the mean frequency of the signal can be related to the transverse flow velocity[8] and is insensitive to the vector nature of the flow and to C_n^2 fluctuation along the path. However this method has its own set of problems that do not arise in the frequency spectrum method described in this report. This technique as well as a "spatial-temporal" probe discussed by Lee[1] will be the subjects of a future investigation.

8. ACKNOWLEDGMENTS

The authors would like to acknowledge the many helpful comments of James Churnside and the valuable contribution of Mildred Birchfield who expertly typed this manuscript.

9. REFERENCES

1. Lee, R. W. (1974): Remote probing using spatially filtered apertures. J. Opt. Soc. Am., 64, 1295-1303.

2. To uniquely identify a transmitter receiver pair, the transmitter elements are pulsed sequentially. The pulses are assumed to be of sufficient duration for a continuous wave approach to be valid. In addition, the time required for a single pulse sequence is assumed to be short compared with the fluctuation time $\tau \simeq (K_o V)^{-1}$ of the received signal where K_o is the resonant wavenumber.

3. Clifford, S. F. (1978): The classical theory of wave propagation in a turbulent medium. In Laser Beam Propagation in the Atmosphere, J. W. Strohbehn, Ed., Springer-Verlag, 9-43.

4. Wang, T. I., G. R. Ochs, and R. S. Lawrence (1981): Wind measurement by the temporal cross-correlation of the optical scintillation. J. Opt. Soc. Am., 20, 4073-4081.

5. Lee, R. W., and J. C. Harp (1969): Weak scattering in random media, with qpplications to remote probing. Proc. IEEE, 57, 375-406.

6. Farmer, D. M., and S. F. Clifford (1986): Space-time acoustic scintillation analysis: A new technique for probing ocean flows. J. Ocean. Eng., OE-11, 42-50.

7. Lawrence, R. S., G. R. Ochs, and S. F. Clifford (1972): Use of scintillations to measure average wind across a light beam. Appl. Opt., 11, 239-243.

8. Lataitis, R. J., L. C. Huff, and S. F. Clifford (1985): Turbulence effects on a rapid precision leveling system. Third International Symposium of the North American Vertical Datum Proceedings, NOAA/National Geodetic Information Center, Rockville, MD., 343-350.

APPENDIX

The signal from each transmitter-receiver pair can be expressed as

$$S_{ij}(t) + \epsilon_{ij}(t) \ , \tag{A1}$$

where $S_{ij}(t)$ is the signal (either the log-amplitude or phase) from the ith transmitter as recorded by the jth receiver in the absence of any noise and $\epsilon_{ij}(t)$ is a random, zero mean noise component. The filtered signal can then be expressed as

$$S_f(t) + \sum_i \sum_j \epsilon_{ij}(t)\ \alpha_i\ \alpha_j \ , \tag{A2}$$

where $\alpha_i(\alpha_j)$ are the transmitter (receiver) coefficients respectively. For uncorrelated noise, the variance of the filtered signal is given by

$$\sigma_f^{\,2} + \sigma_\epsilon^{\,2} \sum_i \sum_j \alpha_i^{\,2}\ \alpha_j^{\,2} \ , \tag{A3}$$

where we have assumed the noise variance associated with each transmitter-receiver is the same and equal to $\sigma_\epsilon^{\,2}$. To include the uncertainty due to finite measurement times we can modify the development of Lataitis et al. [8] to obtain

$$\sigma_f^{\,2} + \sigma_\epsilon^{\,2} \sum_i \sum_j \alpha_i^{\,2}\alpha_j^{\,2} \pm \sqrt{2}\ \sigma_f^{\,2} \sqrt{\frac{2N_0 + 1}{N}} \ , \tag{A4}$$

where N is the total number of samples and N_0 is roughly the number of sampling intervals in the signal correlation time (e.g., for independent samples, $N_0 \to 0$). To obtain Eq. (A4) we have assumed that S_f is a zero mean Gaussian random variable. As a worst case we choose $|\alpha_i| = |\alpha_j| = 1$ and the filtered signal variance can be written as

$$\sigma_f^{\,2} + 16\ \sigma_\epsilon^{\,2} \pm \sqrt{2}\ \sigma_f^{\,2} \sqrt{\frac{2N_0 + 1}{N}} \ . \tag{A5}$$

The measured variance is the sum of three components; the desired variance σ_f^2, a bias $16\,\sigma_\epsilon^2$ due to the noise associated with each transmitter-receiver pair, and an uncertainty $\sqrt{2}\,\sigma_f^2\sqrt{(2N_0 + 1)/N}$ due to finite measurement times. We can define a direct (d) filter SNR as

$$SNR_d \equiv 10\,\log\left(\frac{\sigma_f^2}{16\,\sigma_\epsilon^2 + \sqrt{2}\,\sigma_f^2\sqrt{\frac{2N_0 + 1}{N}}}\right) \qquad \text{(A6)}$$

and a combination (c) filter SNR as

$$SNR_c \equiv 10\,\log\left(\frac{\gamma\,\sigma_{fk}^2 + \delta\,\sigma_{f\ell}^2}{16\,\sigma_\epsilon^2\,(|\gamma| + |\delta|) + \sqrt{2}\,(|\gamma|\,\sigma_{fk}^2 + |\delta|\,\sigma_{f\ell}^2)\sqrt{\frac{2N_0 + 1}{N}}}\right), \qquad \text{(A7)}$$

where σ_{fk}^2 and $\sigma_{f\ell}^2$ represent the filtered variances of the two direct filters used to obtain a combination filter, and γ and δ are the coefficients used in the combination rule shown in Table 2b.

To estimate the expected SNR for the direct and combination filters we have to evaluate σ_ϵ^2, N, N_o, and σ_f^2. The noise variance σ_ϵ^2 can be determined by assuming some SNR for each transmitter-receiver pair. An SNR of 40 dB gives $\sigma_f^2 \simeq 1 \times 10^{-8}$. The signal correlation time is given roughly by $2\pi/(K_0V) \simeq d/V$. For d = 0.6 m, V = 1 m/s, a sampling rate of 10 Hz, and a total sampling time of 20 min, $N_0 = 6$ and N = 12000. The filter signal variance σ_f^2 for an individual filter is given approximately by $\sigma_f^2 = 0.700\,k^2Ld^{5/3}C_n^2A'$, where A' is the area under the path weighting function. For λ = 1.74 cm, L = 660 m, d = 0.6 m, $C_n^2 = 1 \times 10^{-9}\ m^{-2/3}$, $\sigma_f^2 \simeq 0.026\,A'$. The filter whose path weighting function has the smallest area (which corresponds to the smallest variance) will also have the lowest SNR. For the direct filter this corresponds to filter number 4 in Table 1 for which $A' \simeq 0.450$ is the product of the normalization factor and

the normalized area A. Substituting these values into Eq. (A6) yields $SNR_d \simeq$ 13.3 dB as the minimum SNR for the direct filters. The factor limiting the SNR is the uncertainty in the variance due to the finite measurement time. To determine the minimum SNR for the combination filters we first have to verify that the individual filters have a sufficient SNR. The lowest SNR is associated with filter c in Table 2a for which Eq. (A6) yields a SNR of 13.3 dB. The combination filter with the lowest SNR will be filter number 1 in Table 2b because its path weighting function has the smallest area. For this filter the subscripts k and ℓ in Eq. (A7) refer to filters h and a respectively in Table (2a) and the constants γ and δ are 0.76 and -1.11 respectively. Using the appropriate values in Eq. (A7) yields a minimum SNR for the combination filters of 3.5 dB. Once again the uncertainty in the calculated variance due to the finite measurement time limits the SNR.